

The INGV's new OBS/H: Analysis of the signals recorded at the Marsili submarine volcano

Antonino D'Alessandro ^{a,b,*}, Giuseppe D'Anna ^a, Dario Luzio ^b, Giorgio Mangano ^a

^a Istituto Nazionale di Geofisica e Vulcanologia, Roma, Italy

^b Università degli Studi di Palermo, Palermo, Italy

ARTICLE INFO

Article history:

Received 22 September 2008

Accepted 19 February 2009

Available online 5 March 2009

Keywords:

Marsili Seamount

OBS/H

Transient volcano-seismic signals

Continuous volcanic tremor

Polarization analysis

Spectral analysis

ABSTRACT

The ocean bottom seismometer with hydrophone deployed on the flat top of the Marsili submarine volcano (790 m deep) by the Gibilmanna OBS Lab (CNR-INGV) from 12th to 21st July, 2006, recorded more than 1000 transient seismic signals. Nineteen of these signals were associated with tectonic earthquakes: 1 teleseismic, 8 regional (located by INGV) and 10 small local seismic events (non located earthquakes). The regional events were used to determine sensor orientation. By comparing the signals recorded with typical volcanic seismic activity, we were able to group all the other signals into three categories: 817 volcano-tectonic type B (VT-B) events, 159 occurrences of high frequency tremor (HFT) and 32 short duration events (SDE). Small-magnitude VT-B swarms, having a frequency band of 2–6 Hz and a mean length of about 30 s, were almost all recorded during the first 7 days. During the last 2 days, the OBS/H mainly recorded HFT events with frequencies of over 40 Hz and of a few minutes in length. Signals that have similar features in frequency and time domain are generally associated with hydrothermal activity. During the last two days a signal was recorded that had a frequency content similar to that of VT-B events was recorded. It will be referred to as continuous volcanic tremor (CVT). The SDE signals, characterized by a quasi-monochromatic waveform and having an exponential decaying envelope, may have been generated by oscillations of resonant bodies excited by magmatic or hydrothermal activity. By applying polarization and parametric spectral analyses, we inferred that the VT-B were probably multi P-phase events having shallow sources that were situated in narrow azimuthal windows in relation to the positions of the OBS/H. The parametric spectral analysis of the SDE signals allowed us to determine their dominant complex frequencies with high accuracy; these frequencies are distributed in two distinct clusters on the complex plane.

© 2009 Elsevier B.V. All rights reserved.

1. Introduction

In the framework of PRO.ME.TH.E.US (Program of Mediterranean Exploration for Thermal Energy Use), founded by PRAMA s.r.l (Italy), multi-disciplinary research was conducted in the area of the Marsili volcano by Cers-Geo (Centro di Ricerche Sperimentali per le Geotecnologie), University "Gabriele D'Annunzio" of Chieti, the Polytechnic of Bari, ISMAR-CNR (Istituto di Scienze Marine – Consiglio Nazionale delle Ricerche) and INGV (Istituto Nazionale di Geofisica e Vulcanologia). The surveys carried out on the oceanographic CNR's ship *Universitatis* were: multi-beam echo sounding, CHIRP sea bottom profiling, magnetic and gravimetric prospection, measurements of resistivity, temperature, density and some water and rock sampling.

During this experiment, INGV's staff placed a broadband OBS/H (ocean bottom seismometer with hydrophone) on Marsili's flat top (39° 16,383' lat. North, 14° 23,588' long. East) at a depth of 790 m (Fig. 3). It recorded from 12th to 21st July 2006 (D'Anna et al., 2007).

The OBS/H (Fig. 1) was developed by OBSLAB-INGV's staff of Gibilmanna (Palermo), under a project funded by an agreement between the Italian Civil Protection Department and INGV. It was equipped with a Nanometrics Trillium 40 s 3D seismometer and an OAS E-2PD hydrophone, both of which were connected to a Send Geolon MLS digitizer. The signals were sampled at a frequency of 200 samples/s with a 16 bit resolution. The internal clock synchronization to coordinated universal time was made on board ship before the deployment of the OBS/H. The time drift was estimated at below 0.05 ppm, at a temperature between 0–30 °C. The entire deployment sequence from the fall, landing and levelling of the OBS/H to the recording phase, was monitored by the pressure and velocity signals recorded during these phases (Fig. 2).

The first minutes of the recording phase were characterized by very noisy pressure and saturated velocity signals (Fig. 2a, b). During this time the OBS/H was in free fall through a water column of about 790 m. After about 12 min the hydrophone noise decreased remarkably and at the same time the seismometer stopped working (Fig. 2a, b); this coincided with the OBS/H's landing. Several minutes later, the seismometer was freed and started regular signal acquisition with non-zero signal mean value, as the seismometer had not been

* Corresponding author. Via Vincenzo Russo 23, 90121 Palermo, Italy. Tel.: +39 0921 421935; fax: +39 0921 420225.

E-mail address: dalessandro@ingv.it (A. D'Alessandro).

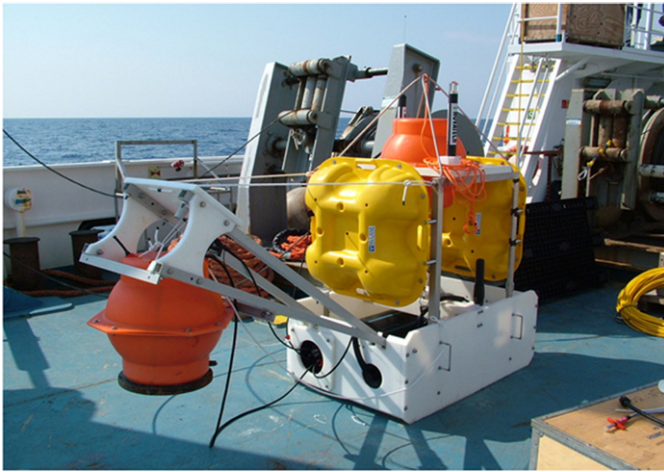


Fig. 1. Temporary seismic station developed by the Gibilmanna OBS Lab (INGV). The OBS/H was equipped with a Nanometrics Trillium 40 s 3D seismometer and an OAS E-2PD hydrophone, both of which were connected to a Send Geolon MLS digitizer.

levelled (Fig. 2b, d). As, the OBS/H was equipped with an auto-leveling system, a few hours later (Fig. 2d) the noise and offset level considerably decreased (**seismometer estimated levelling error less than 0.2°**). A few pulses generated by acoustic commands given by the ship can be seen in the pressure signal (Fig. 2a).

This OBS/H prototype was not equipped with a digital compass, therefore the orientation of the sensor's horizontal components was unknown. It was determined **a posteriori** by polarization analysis of the P phases of well located seismic events (see section Tectonic Events). After nine days of operation ballast was released by an acoustic command, following which the OBS/H surfaced and was recovered.

In this work, after a brief review of the main geological, petrological and geophysical features of the Marsili seamount and

surrounding area, we characterize and classify the events recorded by the OBS/H, by means of spectral and polarization analysis.

2. Geological and geophysical setting

The Tyrrhenian Basin was formed as a consequence of the rifting and back-arc extension of the Alpine–Apennine suture above the north-westerly subducting Ionian oceanic slab (Kastens et al., 1988; Sartori, 2003). The rifting, which started during the Upper Oligocene (28 Ma) in the Southern Tyrrhenian, produced the Vavilov Basin (4.3–2.6 Ma, Sartori, 1989; 8.5–4.5 Ma Argnani, 2000) and the Marsili Basin (1.6 Ma, Kastens et al., 1988; 2.0–1.7 Ma, Argnani, 2000) that are marked by the two volcanoes of the same names. Marsili is, therefore, a back-arc volcano with affinity primarily tholeitic composition (Trua et al., 2004).

With an elevation of about 3000 m above the sea floor, an approximate length of 60 km in a NNE–SSW direction and a mean width of 16 km, this seamount is the biggest European volcano (Marani and Gamberi, 2004). Fig. 3 shows the shaded relief bathymetric map of the Marsili basin and the OBS/H deployment point (Marani and Gamberi, 2004).

Several authors have constructed geophysical models of the lithosphere of the Southern Tyrrhenian Basin (Marani et al., 2004 and reference contained therein; Piromallo and Morelli, 2003; Panza et al., 2004, 2007; Montuori et al., 2007; Calò et al., 2009) which have provided information about the Marsili Basin's role in the geodynamic evolution of the Tyrrhenian Sea.

The main structure highlighted in these tomographies is a high velocity body, having an average thickness of about 250 km, which dips steeply ($\approx 70^\circ$) in a NW direction down to more than 400 km. This body is unanimously ascribed to the Ionian lithospheric slab subducting under the Tyrrhenian Basin.

Calò et al. (2009) and Panza et al. (2004) found low V_p and V_s bodies under the Marsili volcano, above the high velocity layer related to the upper part of the Ionian subducting slab. This low velocity body

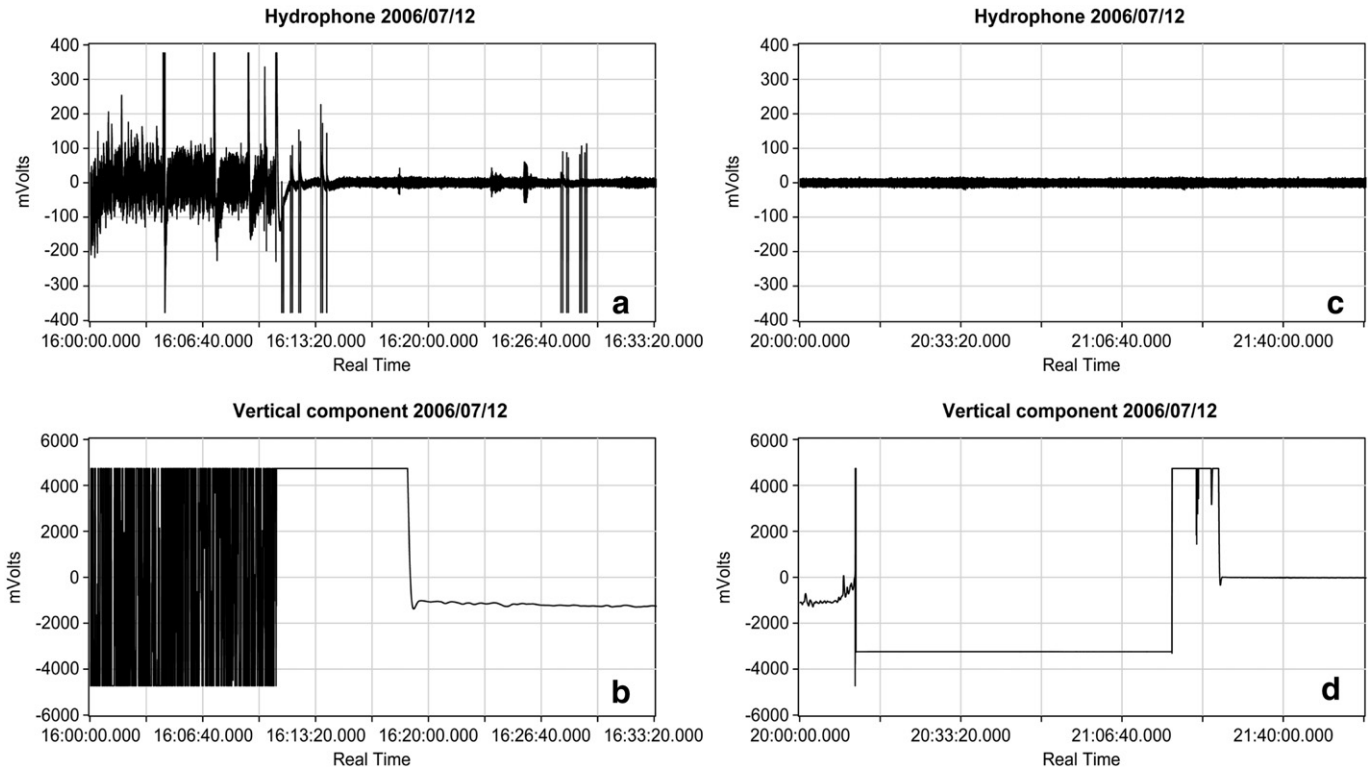


Fig. 2. Unfiltered signal intervals recorded by the hydrophone and the vertical component of the seismometer during the fall and landing of the OBS/H (a, b) and during the levelling phases (c, d).

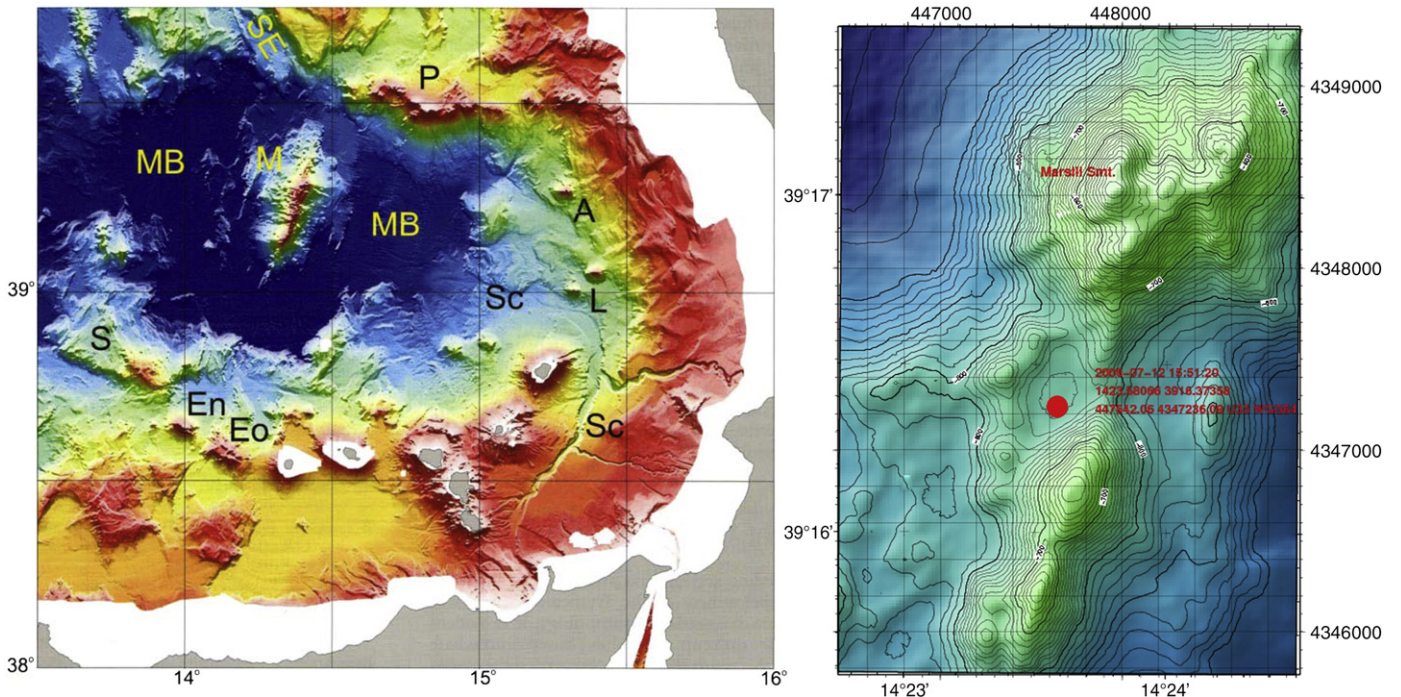


Fig. 3. Shaded relief bathymetric maps of the Marsili basin Province (Marani and Gamberi, 2004) and Marsili flat top: Marsili basin (MB) is the recent-most ocean crust floored basin, characterised by the large, axially located Marsili volcano (M). The red circle indicates the OBS/H deployment point.

provides evidence of the accumulation of significant amounts of mantle partial melts (some thousands of km³) that likely feed the present-day volcanic activity.

Zito et al. (2003) compiled a heat flow map of the Tyrrhenian Sea and surrounding areas. This map shows a very high regional mean value of 120 mW m⁻² with a local maximum of 245 mW m⁻² centred on Marsili. This maximum was attributed both to recent tectonic and volcanic activity and to probable convective water movements (Mongelli et al., 2004).

The regional magnetic anomaly field of the Marsili Basin displays a general spreading of the basin (Faggioni et al., 1995; Nicolosi et al., 2006) and suggest that between 1.6 and 2.1 Ma spreading took place at the remarkable rate of about 19 cm/yr.

Beccaluva et al. (1982) and Marani et al. (1999) collected some rock samples from Marsili Basin that had undergone a strong degree of hydrothermal alteration.

On the basis of all the geophysical, geological and petrological information obtained, Marsili volcano can be considered as being the key needed to understand the dynamics of spreading and back-arc lithosphere formation in this Tyrrhenian sector.

3. Data analysis

During this experiment, more than 1000 seismic events were recorded which could be classified as tectonic or volcanic (D'Alessandro et al., 2006, 2007, 2008). Several high frequency wave trains, clearly associated with anthropic activity (mainly ships in transit above the OBS/H), were also recorded.

Due to the complex nature of volcanic processes, a great variety of distinct seismic signals are often observed. Almost all the events recorded by the OBS/H can be ascribed to magmatic movements or hydrothermal activity of Marsili. We classified the recorded events on the basis of the large amount of literature available on this topic as follows.

Pioneering work on the classification of volcano-seismic signals was effected by Minakami (1960) followed by more recent works of McNutt (1992, 1996, 2000, 2005), Chouet (1996, 2003), Zobin (2003),

For our analysis we follow the classification of the volcano-seismic signals reported on Wassermann (2002).

During the entire 9 days' record, we identified 4 classes of signals: CVT (continuous volcanic tremor), HFT (high frequency tremor), VT-B (volcano-tectonic events, B type) and SDE (short duration events).

For all the signals, the instruments' transfer functions were deconvolved and their amplitudes were corrected to velocity (m/s) for the seismometer and pressure (microbar) for hydrophone. For each 1 h interval, we also used a least square regression to remove the linear trend. Finally, we applied the rotation matrix estimated from polarization analysis applied to the tectonic earthquakes located by INGV to the velocity signals, to determine the NS and EO components. All the algorithms used for data analysis are described in the following section.

3.1. Methods

In this paper the power spectral density (PSD) was calculated by a variation of the periodogram method, known as the Welch method or periodogram averaging (Welch, 1967). To analyze the time variation of the signal frequency content, we utilized a time-frequency analysis with fixed resolution both in time and frequency domains, that is the spectrogram method or short time Fourier transform (STFT, Bartosch and Seidl, 1999).

Most of the methods used to characterize the polarization of a vectorial wave in the time domain are based on the eigen-analysis of the covariance matrix G_{ij} (Flinn, 1965)

$$G_{ij} = \begin{bmatrix} \text{Var}(Z) & \text{Cov}(Z, N) & \text{Cov}(Z, E) \\ \text{Cov}(N, Z) & \text{Var}(N) & \text{Cov}(N, E) \\ \text{Cov}(E, Z) & \text{Cov}(E, N) & \text{Var}(E) \end{bmatrix}$$

where $\text{Var}()$ and $\text{Cov}()$ indicate the variance and covariance of Z=vertical, N=north-south and E=east-west components of the seismic signal. The solution of the simultaneous equations

$$(G_{ij} - \lambda I_{ij})u_j = 0$$

where I_{ij} is the identity matrix, allows one to determine the unitary vectors u_j , $j = 1, 2, 3$ relative to the three polarization principal directions and the corresponding eigenvalues $\lambda_1 \geq \lambda_2 \geq \lambda_3$.

The polarization characteristics of the ground motion, is defined by the linearity index and the azimuth and dip of the main polarization direction (Flinn, 1965). Classical polarization analysis assumes that the signal is noise free, nevertheless the 3D record includes both signal and noise and the polarization analysis is reliable only if the signal to noise ratio is very high. To statistically improve the estimation of the polarization attributes, we applied a noise correction to the covariance matrix. This correction is based on the assumption that in the selected window the noise can be regarded as a stochastic process, stationary both in time and space domains. Okada (2003) showed that seismic noise can be regarded as a stationary process up until a few hours and kilometres. We also presume that a generic component of the signal can be considered uncorrelated to noise. Under this assumption we can write:

$$\text{Var}(S_x + R_x) = \text{Var}(S_x) + \text{Var}(R_x) + 2\text{Cov}(S_x, R_x) = \text{Var}(S_x) + \text{Var}(R_x)$$

and

$$\begin{aligned} \text{Cov}((S_x + R_x), (S_y + R_y)) &= \text{Cov}(S_x, S_y) + \text{Cov}(S_x, R_y) + \text{Cov}(R_x, S_y) + \text{Cov}(R_x, R_y) \\ &= \text{Cov}(S_x, S_y) + \text{Cov}(R_x, R_y) \end{aligned}$$

where S_x and R_x are generic signal and noise components respectively. We can now define a new covariance matrix G'_{ij}

$$G'_{ij} = G_{ij} - R_{ij}$$

where R_{ij} is the covariance matrix of a signal interval, containing only noise, very close to the signal window analyzed. So G'_{ij} can be used instead of G_{ij} to determine the polarization characteristics of the ground motion.

The polarization analysis before described does not take in account that the polarizations vary as a function of frequency as well as time, and thus variations seen in the time domain could be due to changes in the frequency content of the signal. In order to avoid this problem the seismograms are usually band-pass filtered in the frequency range of interest, but generally this is not the most efficient way to measure these variations. For this reason we implemented a frequency-time polarization analysis by mean of the Fourier transform of the 3-C signal.

Vectorial signals can be represented as the superposition of harmonic oscillations in the x -, y -, and z -directions, which for each frequency trace out an ellipse in the space. For each frequency the information contained in the Fourier coefficient of the three components can be re-expressed as geometrical parameters of the ellipse. The geometrical parameters of the ellipse that we consider here are the flattening and the tilt and the azimuth of its major axis. Flattening is defined as

$$\text{flattening} = 1 - \left(\frac{b(f)}{a(f)} \right)$$

where $a(f)$ and $b(f)$ are the major and minor axes of the ellipse respectively. The tilt is the angle that each ellipse's major axis makes with the vertical while the azimuth is the angle between the projection of the major axis on the horizontal plane measured counter-clockwise from the N. The expressions to calculate the ellipse geometrical parameters from complex Fourier coefficients are those proposed by Pinnegar (2006) for the S transform coefficients. The time dependence of this spectra is investigated by means of a sliding window.

We model the SDE as transiently excited eigen-oscillations of a body having a finite length scale, embedded in a infinite, homogeneous, elastic medium (Nakano et al., 1998). We used the tails of exponentially decaying harmonic waveforms ($e^{i2\pi(f-ig)t}$) to determine the characteristic complex frequency of each SDE using the Sompi method (Yokoyama et al., 1997). The method is based on an

inhomogeneous autoregressive (AR) model of a linear dynamic system, in which the excitation is assumed to be a time-localized function applied at the beginning of the event (Nakano et al., 1998). When the excitation equals zero the inhomogeneous AR equation becomes homogeneous. To study the solution of the homogeneous equation the onset inhomogeneous portion of the seismogram is ignored.

3.2. Tectonic events

The OBS/H recorded 19 tectonic events, of which are: 1 teleseismic event, 8 regional events (located by INGV) and 10 small local events (non located earthquakes). The teleseismic event was the $M_S = 7.2$ earthquake that took place in Java on 17th July 2006 (Fig. 4a). Fig. 4b shows the vertical component of a local tectonic event band-pass filtered between 1.5 and 12 Hz.

The epicentres of the regional events were distributed on a wide azimuthal range in respect of the station (Fig. 4c); their hypocentral depth was between 5 and 132 km, while the local magnitude was between 2.3 and 3.3. The regional events were used to estimate the azimuthal orientation of the seismometer's horizontal components through the polarization analysis of the P phases. We compared the azimuth from each event to the station (y) with the corresponding azimuth of the calculated polarization direction (x).

The sensor orientation was then determined by least square regression between the x and y , using the relationship $y = mx + q$ (Fig. 4d). In this equation $\varepsilon = \hat{m} - 1$ could be linked to systematic errors in the x and y data, while \hat{q} value measures the angle between the sensor's horizontal axis and the NS and EO directions. The estimate \hat{m} is very close to 1 while \hat{q} is +144.7° with 95% confidence interval equal to [133.4°–156.0°].

3.3. Seismic noise and volcanic tremor

Volcanic and geothermal activity often generate tremor with various characteristic peaks in its seismic spectrum, continuous volcanic tremor (CVT). The characterization of CVT in marine areas is generally difficult because the surface of the sea is a powerful source of broadband hydro-acoustic noise which is superimposed on it. To analyze the frequency components of the noise and their time variations we calculated (PSD) and the STFT.

In order to calculate the PSD we divided the signal into 80 s long intervals (16,000 samples) with an overlap of 40 s, applied a Hanning window to each interval and used the FFT. To compare the PSD of the noise recorded on Marsili with both Peterson's (1993) land high noise model (HNM) and a low noise model (LNM), defined for vertical component, we transformed a noise record without any event (about 40 h) into acceleration.

Fig. 5 shows the most significant differences between the HNM and LNM (Peterson, 1993) and the PSD for the deployment at Marsili. The pressure PSD is also represented in the same figure. The very high seismic noise level at low frequency is probably caused by large scale sea currents or low-frequency sea waves (Webb, 1998). The double spectral peak near 0.2 Hz was caused by sea waves that mostly propagate as the fundamental mode of Rayleigh waves while the peak at about 0.6 Hz could be attributed to interference of sea waves (Webb, 1998).

The wide peak of between 2 and 5 Hz is probably related to volcanic activity. In fact, this frequency band coincides with the main frequency band of the VT-B events. Furthermore, during the nine days of recording we recognized a transition from VT-B events at short intervals to a continuous signal (in the last two days). A similar phenomenon was observed during several cycles of increased volcano-seismic activity at Montserrat volcano (Neuberg et al., 2000).

In the narrow frequency range of 1.5–3 Hz, the pressure PSD is characterized by a local maximum that could hide the 2–5 Hz peak observed in the acceleration PSD. Moreover, the seismic noise with frequency above 5 Hz has a very high amplitude. Sharp peaks in this

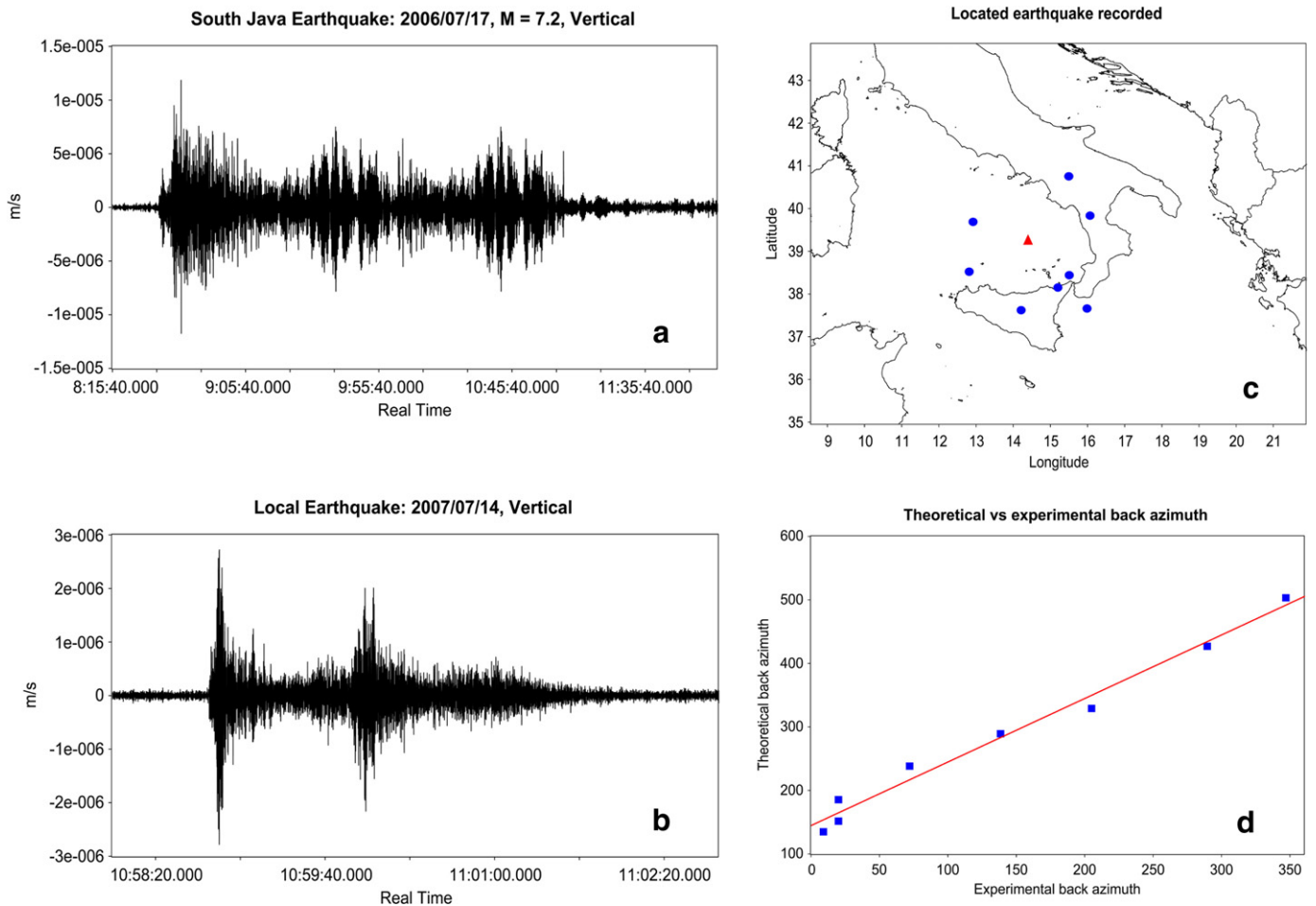


Fig. 4. Vertical component of: (a) Java event of 2006/07/17, $M_s = 7.2$ (low-pass filter with cut-off frequency 2.5 Hz) and (b) local earthquake (band-pass filter with cut-off frequencies 1.5 and 12 Hz); (c) map of the regional earthquakes' epicentres; (d) regression line between epicentral azimuths estimated from earthquake location and polarization analysis.

frequency range are often ascribed to overtones of fundamental modes with frequency between 0.5 Hz and 7 Hz (Konstantinos and Schindlwein, 2002). However, the high level of the noise, mostly controlled by wave breaking (McCreery et al., 1993) and man-made sources (Wenz, 1962), makes it difficult to extract the volcanic component from the noise.

In order to analyse the variations in the frequency and time domains of the noise amplitude, we calculated the STFT, using a sliding window of 20 s (4000 samples) and an overlapping of 3800 samples. A spectrogram of seismic noise recorded in the last two days is shown in Fig. 6. The CVT's main peaks are characterized by nearly stationary amplitude on the entire record.

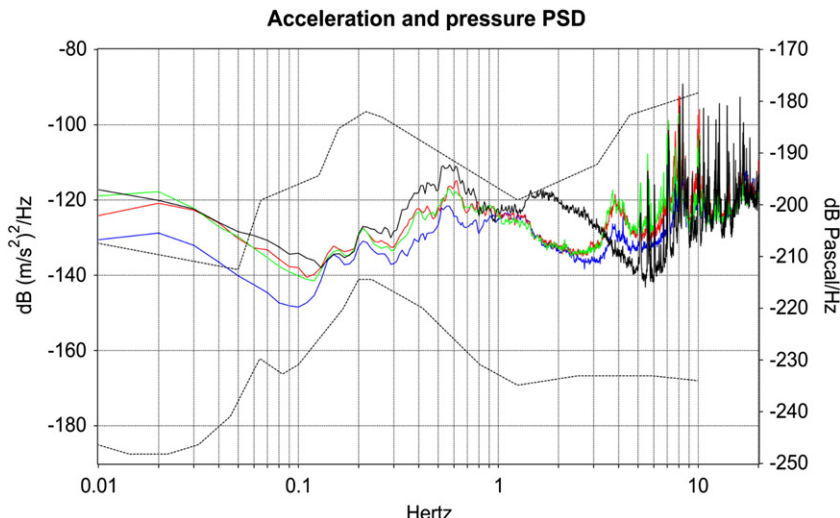


Fig. 5. Acceleration and pressure PSD of noise recorded on Marsili; blue = vertical, red = north-south, green = east-west, black = pressure, grey = Peterson low and high noise models (1993). The wide peak of between 2 and 5 Hz coincides with the main frequency band of the VT-B events and is probably related to volcanic activity.

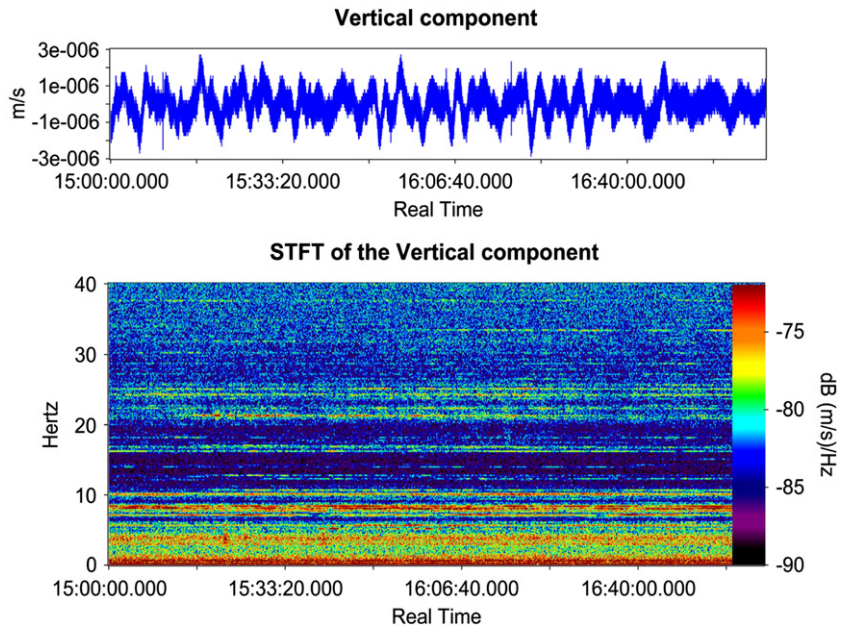


Fig. 6. Unfiltered noise (vertical component) with and relative spectrogram. The CVT's main peaks, recognizable in the 2–5 Hz frequency band of the spectrogram are characterized by nearly stationary amplitude on the entire record.

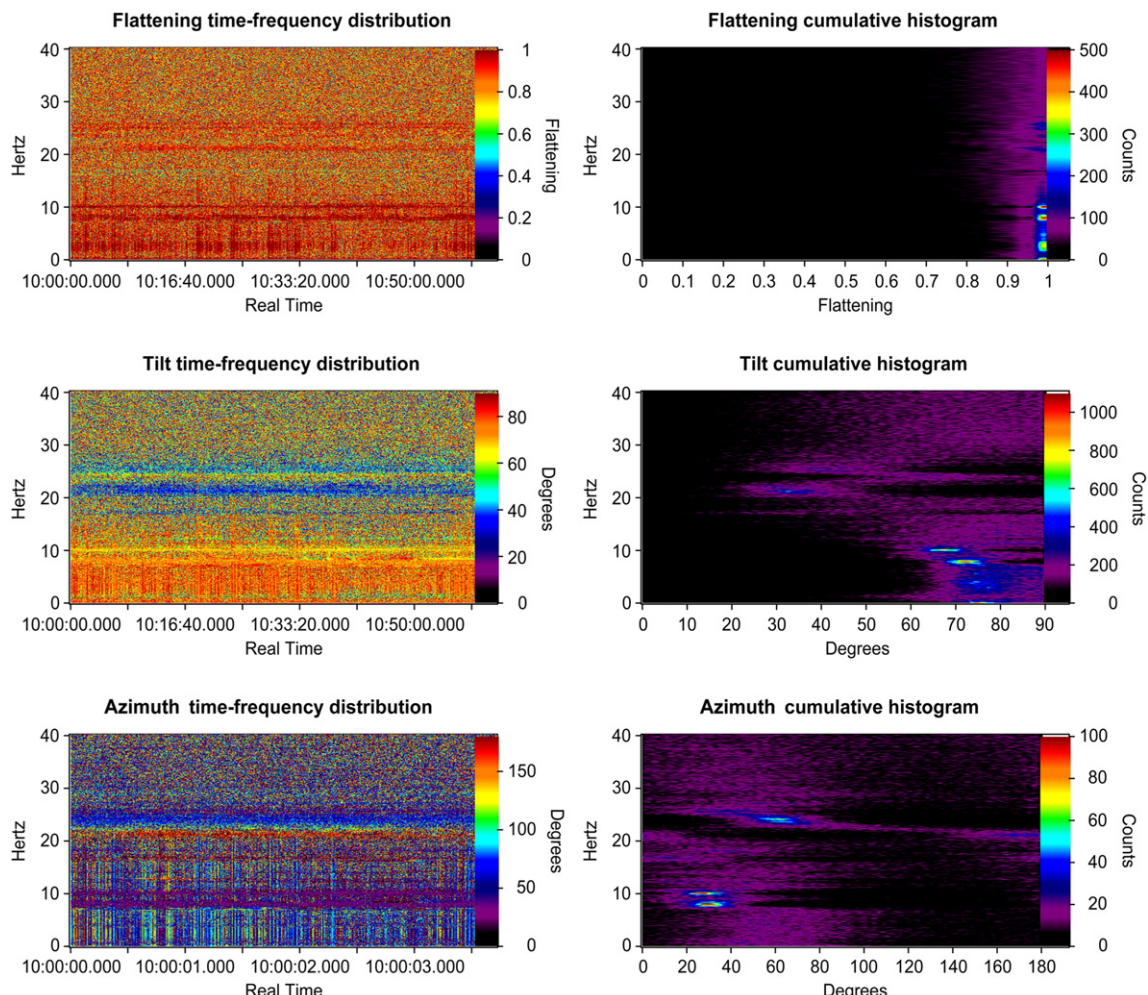


Fig. 7. Time–frequency distributions of the polarization attributes and relative time cumulative histograms. See text comments.

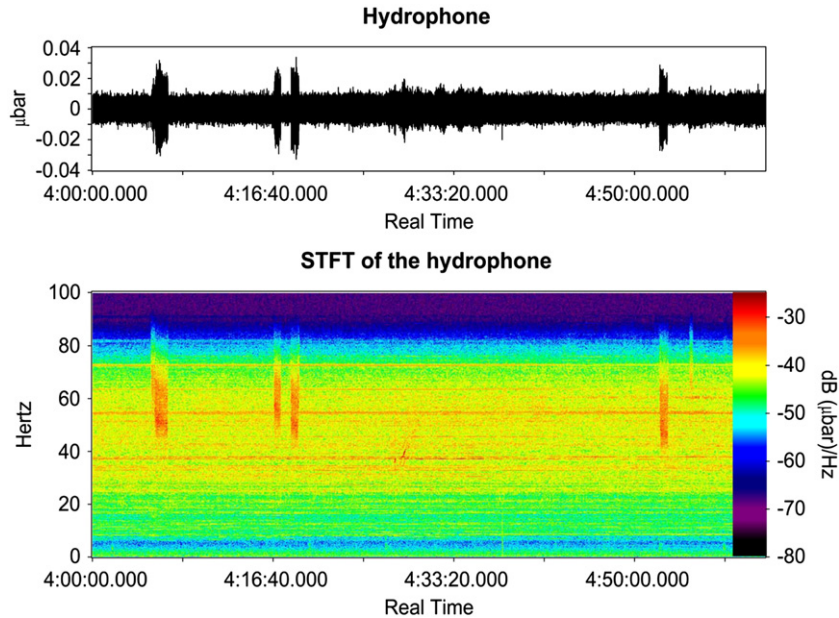


Fig. 8. Unfiltered noise (pressure signal) with HFT bursts recognizable in time and frequency domains. The HFT has a boxcar envelope with sudden beginning and ending, a time duration of a few minutes and a dominant frequency of between 40 and 90 Hz.

To make a guess at the nature of the sources of CVT in the Marsili area, we applied a time–frequency polarization analysis to the vectorial signal. The geometrical elements determined were: the length of the ellipse axis and the tilt and azimuth of the major axis. The time variations of these parameters were observed and then determined by means of a sliding window. Like STFT, we used a sliding window of 20 s (4000 samples) and an overlapping of 3800 samples. Fig. 7 shows the time–frequency distribution of the polarization attributes and the relative time cumulative histograms.

The wave polarization is nearly linear in narrow frequency intervals centred at about 2.6, 8.0, 10.1 Hz. The time cumulative histogram of the flattening shows a statistical predominance of linearly polarized waves, probably to be referred to waves that

travelled through the water layer. The wavefield is also characterized by a prevalence of large tilt angles, while small tilt angles are only observable in the frequency range 20–27 Hz. In the three frequency intervals, where the polarization is nearly linear, the histograms of the tilt angles are unimodal and very sharp around 75°, 72° and 63° respectively. The azimuth histograms don't show any systematic trend in frequency domain; only three sharp peaks are evident around 8.0, 10.1 and 24.4 Hz and a smooth peak below 8 Hz. The first two frequencies have similar azimuth, about 35°, while the low frequencies show an azimuth between 40° and 75°.

The pressure signal recorded in the last two days of the experiment shows the occurrence of a HFT (159 HFT events). Fig. 8 shows a signal portion containing some HFT bursts and the relative spectrogram. The

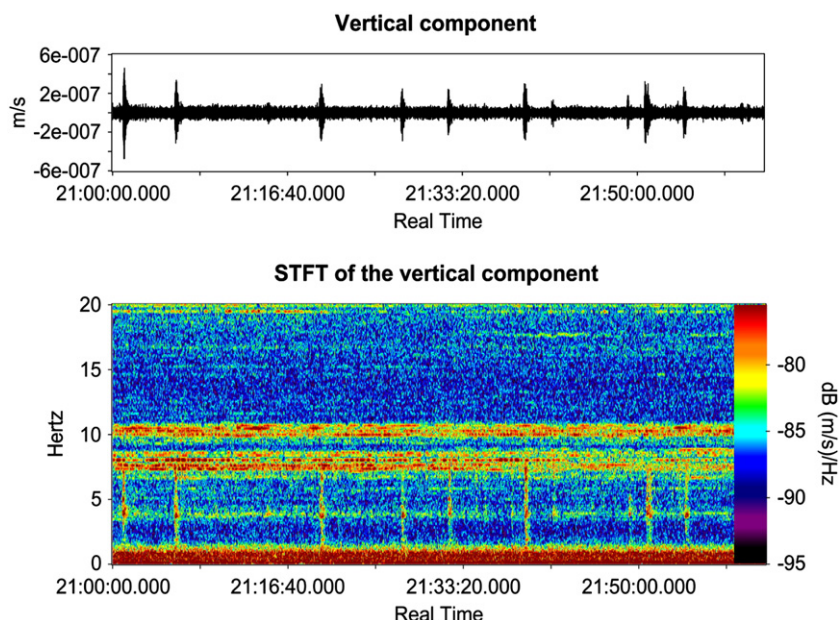


Fig. 9. Example of signal (vertical component) and relative spectrogram containing a VT-B swarm. The signal is filtered in the band 2.0–7.0 Hz while the spectrogram refers to the unfiltered signal.

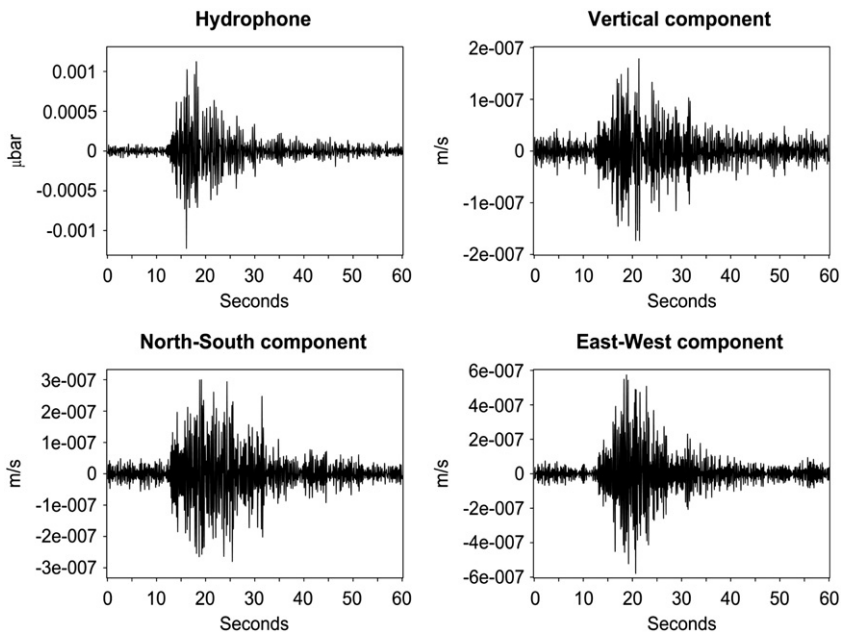


Fig. 10. Example of VT-B event (signal filtered in the band 2.0 and 7.0 Hz). The VT-B events had a mean length of about 30 s and were characterized by emergent and low-amplitude onsets of P phases. They often did not show any clear S phase arrival.

HFT has a boxcar envelope with sudden beginning and ending, a time duration of a few minutes and a dominant frequency of between 40 and 90 Hz. Similar signals were recorded at the Satsuma-Iwojima

hydrothermal system (Ohiminato, 2006) and ascribed to sudden vapour emission from water-filled underground pockets when the water temperature exceeded the vaporization point.

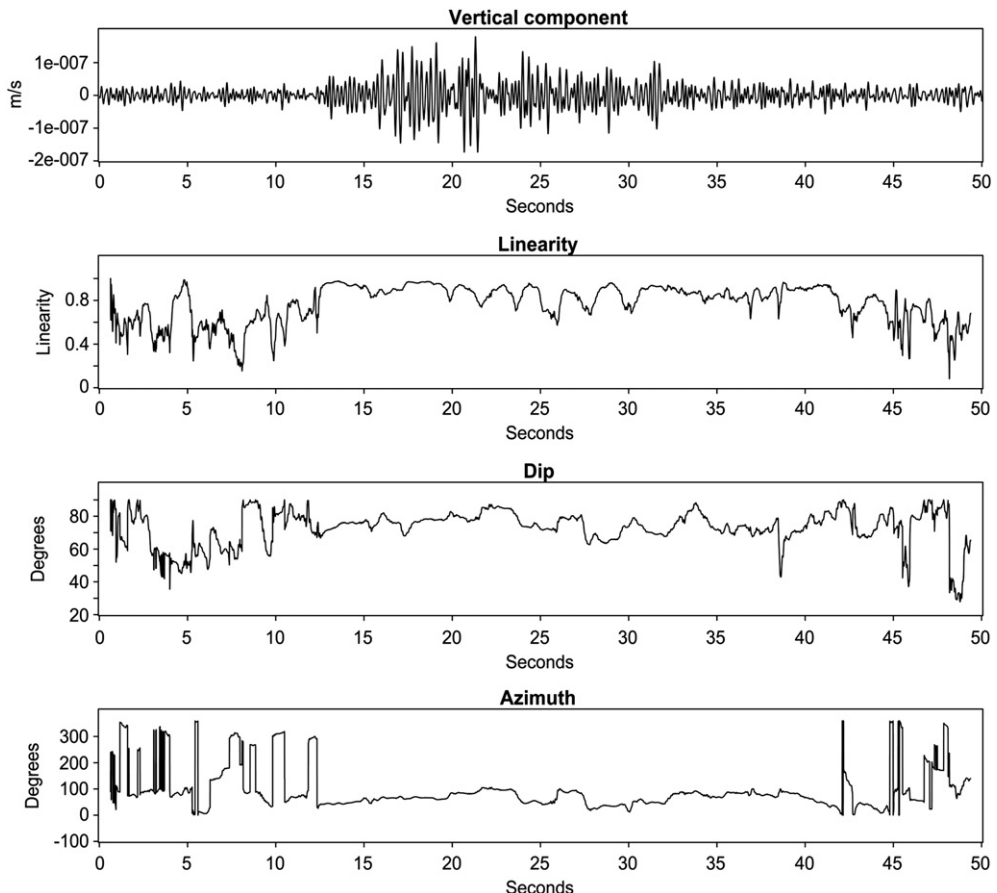


Fig. 11. Time domain polarization analysis of a VT-B event (sliding window length 1.25 s, 250 samples). The highly linear beginning of the analyzed traces was probably caused by body wave dominance while brief decreases in the linearity probably indicate the arrivals of new body wave phases. Dip and azimuth of each event show small time variations, generally coincident with the short drops in linearity. The dip vary between 60° and 90° and exhibit jumps variations less than 15° wide, while the discontinuous variations of the azimuth are less than 60° wide.

3.4. Volcano-tectonic events

Most of the events recorded on Marsili (817) were classified as VT-B (Wassermann, 2002). Their average recurrence time was very short (about 10 min) in the first 5 days, although afterwards the recurrence frequency quickly decreased down to less than 10 events per day.

Fig. 9 shows a one-hour record of the velocity vertical component and its amplitude spectrogram containing a VT-B swarm, while Fig. 10 shows a single VT-B event, filtered in the frequency band 2.0–7.0 Hz, where most of the energy was concentrated. The waveform analysis shows that the VT-B events had a mean length of about 30 s and were characterized by emergent and low-amplitude onsets of P phases. However, they often did not show any clear S phase arrival.

We carried out a time domain polarization analysis of each VT-B event. In order to optimize this analysis we used continuous sliding windows about 5 times the main period (1.25 s, 250 samples). To improve the estimates of the polarization attributes, the covariance matrix was corrected for the effects of the noise as described in Section 3.1.

The highly linear beginning of the analyzed traces was probably caused by body wave dominance (Fig. 11). Brief decreases in the linearity probably indicate the arrivals of new body wave phases. The angles between the main eigenvector and the vertical direction (dip)

and that between the main eigenvector's horizontal component and the N direction (azimuth) of each event show small time variations, generally coincident with the short drops in linearity. The dip vary between 60° and 90° and exhibit jumps variations less than 15° wide, while the discontinuous variations of the azimuth are less than 60° wide. The polarization analysis results suggest that the VT-B events were probably a superimposition of body waves coming from shallow sources (Wassermann, 2002).

The polarization in the horizontal plane was determined for the 220 VT-B events having the highest signal to noise ratios. The back-azimuth of these events, coincident with the horizontal component of the wave vector was determined by polarization analysis of the first arrivals ascribed to up-going P-waves. Under this assumption the sign of the cosine of the angle between the main polarization direction and the vertical is used to resolve the π ambiguity of the azimuth. The back-azimuths so estimated were used to construct a cumulative histogram with bin width of 10°. Fig. 12 shows the rose diagram representation of this histogram. It clearly displays two main directions in the NE quadrant. Considering the uncertainty in the estimation of main polarization direction and the fact that data have been recorded by unique sensor, it is difficult to ascribe the two maximum frequency directions to a presence of distinct seismogenic volumes.

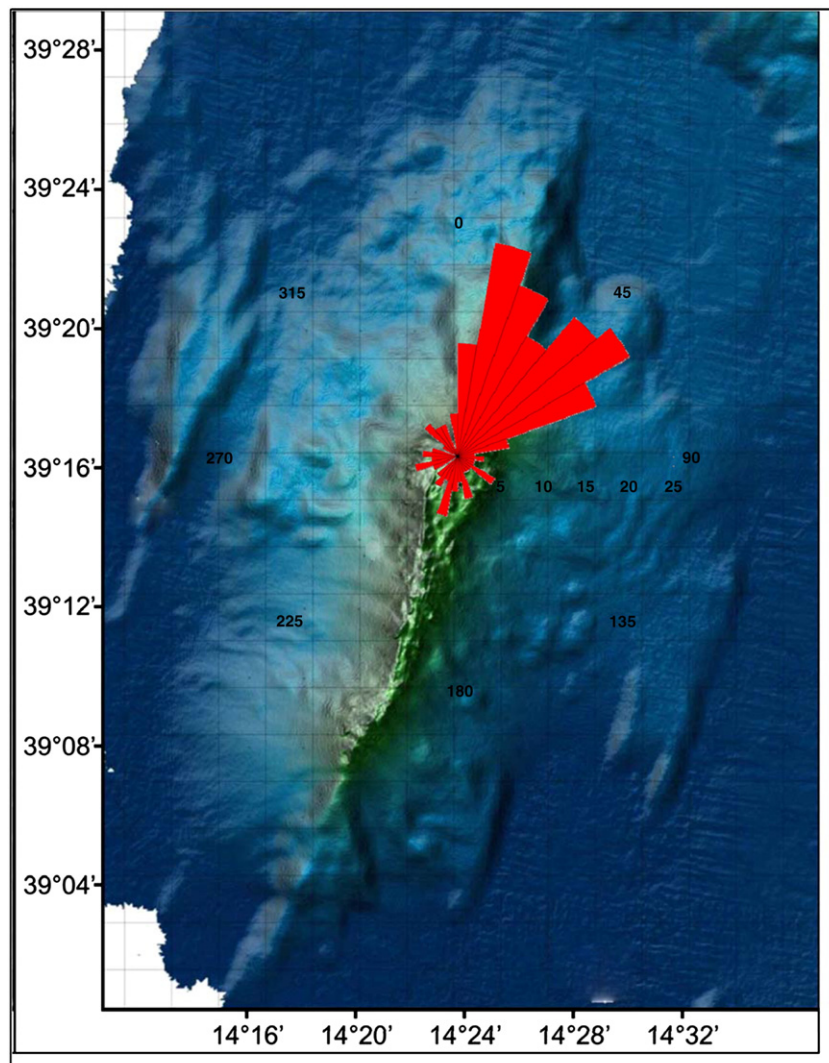


Fig. 12. Rose diagram representation of the cumulative histogram, with bin width of 10°, of the back-azimuths estimated for 220 VT-B events having the highest signal to noise ratios. It clearly displays two main directions in the NE quadrant.

3.5. Short duration events

Several dozen events recorded on the Marsili volcano had a frequency spectra with only one or two narrow main peaks, usually

around 7.5 Hz, an exponential decay of the signal amplitude, generally impulsive onsets and durations between 2.5 and 4 s.

Similar waveforms are often recorded in volcanic and hydrothermal areas. These events are called **tornillo** (Seidl et al., 1999) or

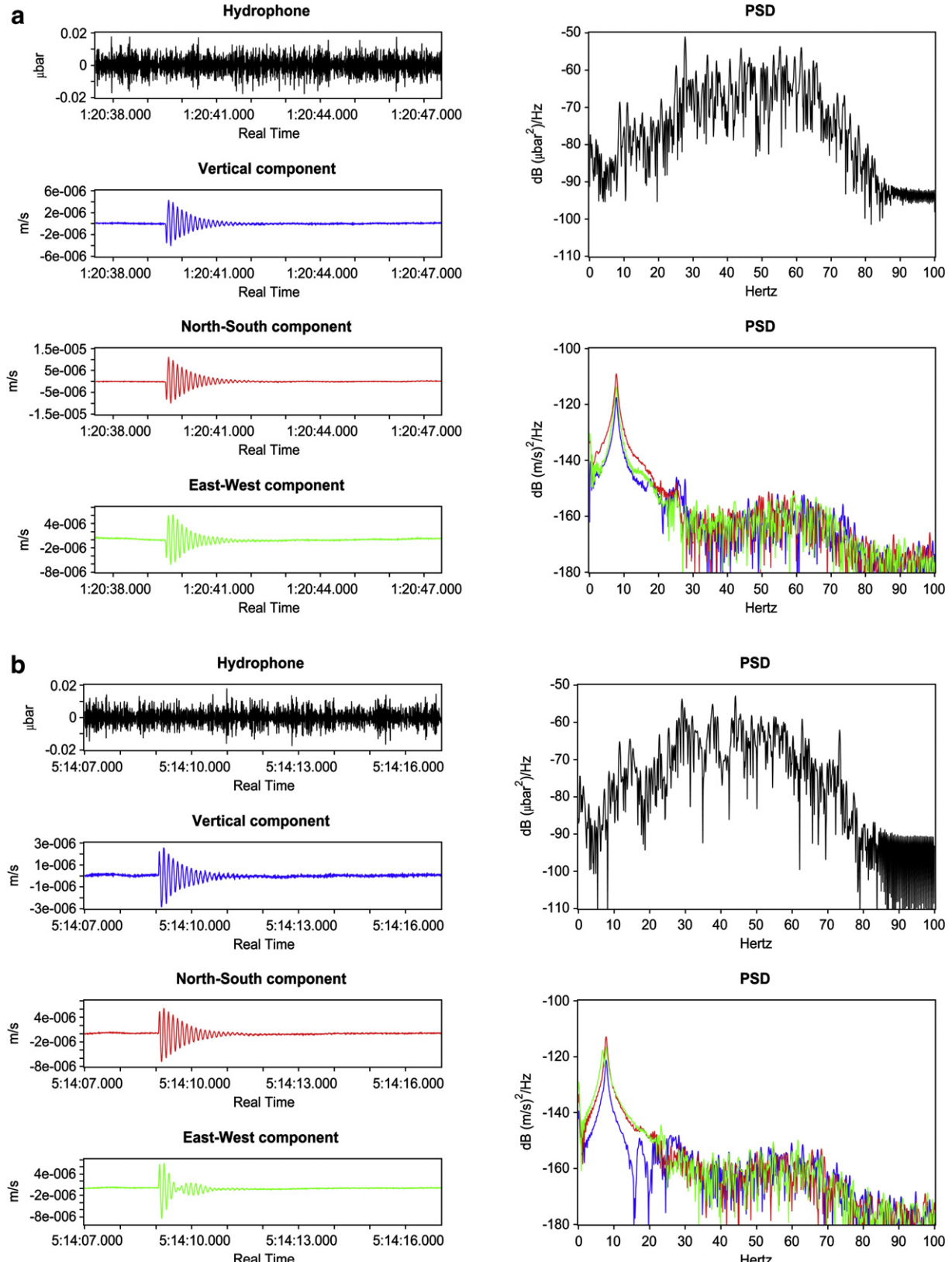


Fig. 13. Examples of SDE recorded on Marsili: (a) quasi-monochromatic SDE; (b) SDE with splitting of the main spectral peak on the east–west component; (c) SDE with a high frequency phase also recorded by the hydrophone.

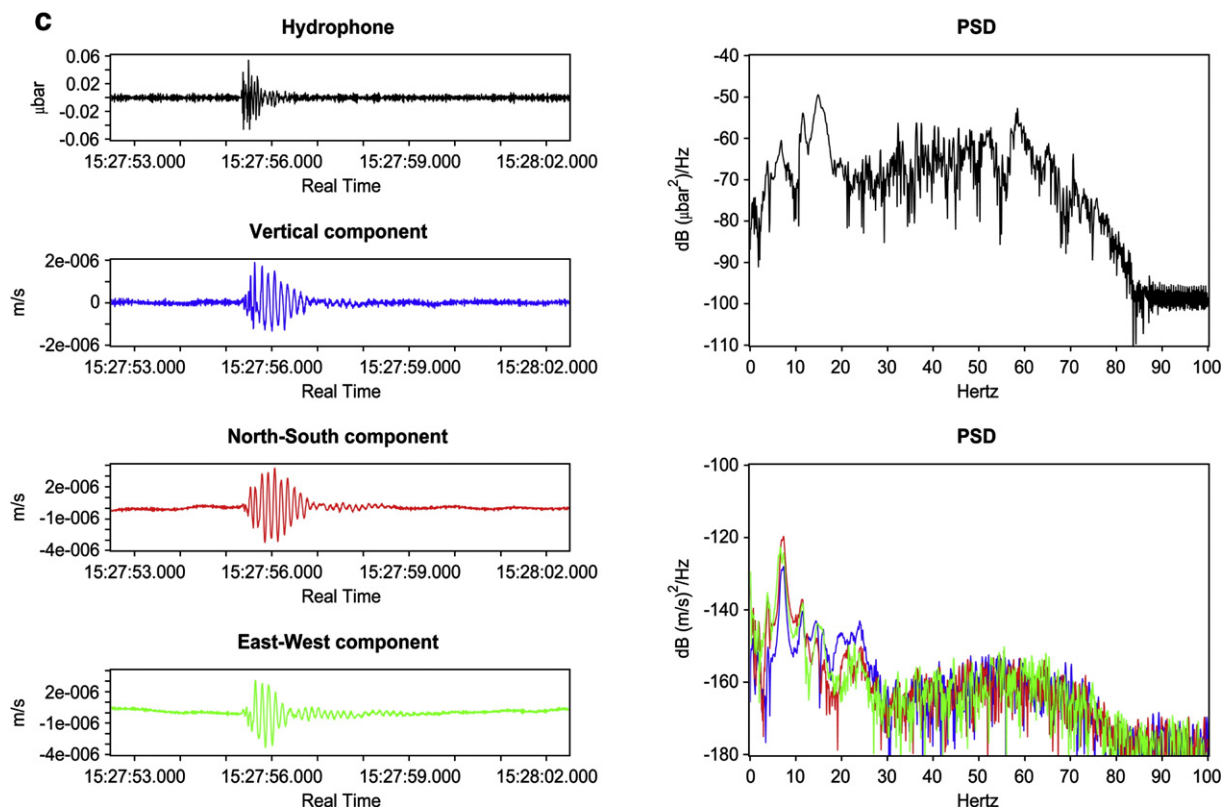


Fig. 13 (continued).

monochromatic event (Montaldo, 1993) or Long Period Event (Nakano et al., 1998) or short duration event (Diaz et al., 2007) depending on their spectral content and damping characteristics. Events of this nature can be generated by oscillations of a resonant body excited by magmatic or hydrothermal activity (Chouet, 1996).

Very similar waveforms have also been recorded recently at La Fossa (Alparone et al., 2008) and by OBS in non volcanic areas such as the Galicia Margin, North Atlantic Ocean (Diaz et al., 2007).

Due to their low energy, these events can only be recorded near the source. In view of the close likeness between our signals and those

recorded in the North Atlantic Ocean (Diaz et al., 2007), we called them SDE (short duration event).

We separated the total set of SDE into three homogeneous subsets on the basis of several parameters. The first subset exhibited a quasi-monochromatic behaviour in each velocity component (9 events, Fig. 13a), the events of the second subset showed, at least for one component, the splitting of the main spectral peak (16 events, Fig. 13b), while the events of the third subset had a high frequency phase that had also been recorded by the hydrophone (7 events, Fig. 13c).

Nakano et al. (1998) model the SDE as transient waves excited by the normal modes of vibration of a resonator. In order to estimate their characteristic complex frequencies (f , g) and improve the frequency spectra resolution, we applied the Sompi method (Nakano et al., 1998) that is based on the analysis of the tail of an exponentially decaying harmonic wave.

By plotting them on the complex plane (Fig. 14) we identified two distinct clusters that had the following mean complex frequencies: $f_1 = 7.8 \text{ s}^{-1}$, $g_1 = -0.35 \text{ s}^{-1}$ and $f_2 = 7.5 \text{ s}^{-1}$, $g_2 = -0.47 \text{ s}^{-1}$ with standard deviation $\sigma_{f1} \approx \sigma_{f2} = 0.17 \text{ s}^{-1}$, $\sigma_{g1} \approx \sigma_{g2} = 0.02 \text{ s}^{-1}$. These two clusters were probably linked to two similar but distinct fluids resonating processes.

The polarization analysis shows a high degree of linearity (flattening > 0.8) of most of the SDE analysed; in particular the signals of the first subset have a linearity index of almost one (Fig. 15). The dip of the main eigenvector of the SDEs are always between 65° and 80°, while the azimuth distribution does not show any clear preferential direction.

4. Conclusions

During the experiment conducted in July 2006, an OBS/H was deployed on the flat top of the Marsili submarine volcano. More than 1000 seismic events were recorded in only 9 days.

Throughout the first seven days, Marsili's seismic activity was characterized by the occurrence of a swarm of VT-B, the intensity of

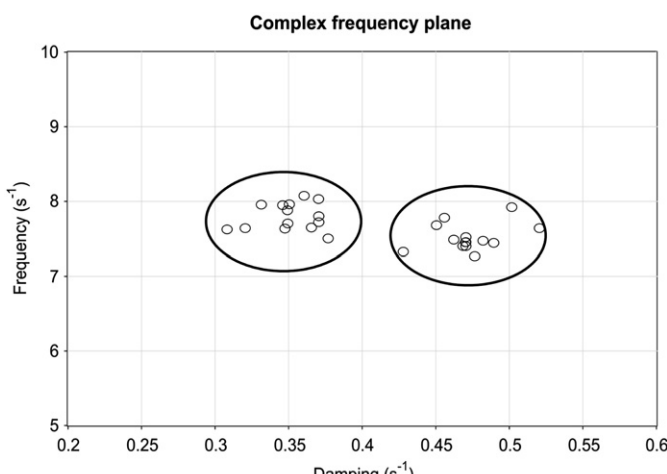


Fig. 14. Plotting of the SDE complex frequencies estimated using the Sompi method. The ellipses indicate the two distinct clusters identified that had the following mean complex frequencies: $f_1 = 7.8 \text{ s}^{-1}$, $g_1 = -0.35 \text{ s}^{-1}$ and $f_2 = 7.5 \text{ s}^{-1}$, $g_2 = -0.47 \text{ s}^{-1}$ with standard deviation $\sigma_{f1} \approx \sigma_{f2} = 0.17 \text{ s}^{-1}$, $\sigma_{g1} \approx \sigma_{g2} = 0.02 \text{ s}^{-1}$.

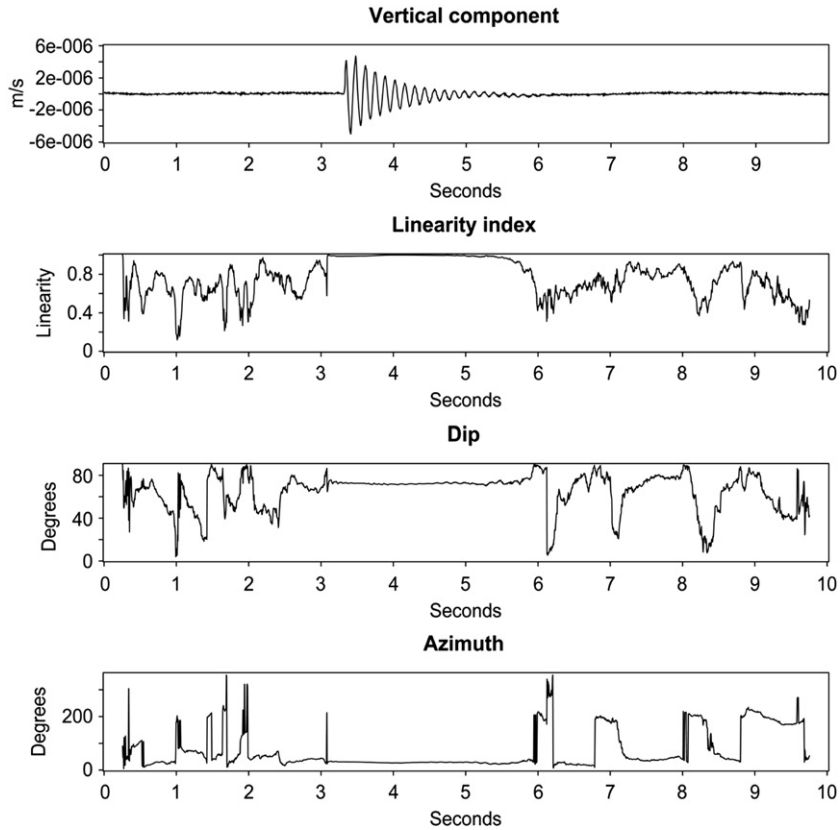


Fig. 15. Example of time domain polarization analysis of an SDE. The polarization analysis shows a high degree of linearity (flattening >0.8) of most of the SDE analysed. The dip of the main eigenvector of the SDEs are always between 65° and 80° , while the azimuth distribution does not show any clear preferential direction.

which drastically decreased during the last two days (Fig. 16). In fact, the last two days were instead characterized by a continuous volcanic tremor, having the same spectral content and similar azimuth of the VT-B, and by a scattered occurrence of high frequency tremor (Fig. 16). During the 7th day a variation in the volcano-seismic activity occurred. It is our belief that during these last 2 days an increase in the volcanic activity reduced the time lags between the VT-B events generating the CVT, as at Montserrat (Neuberg et al., 2000).

At the same time, the signals were affected by some HFT bursts, very similar in time and frequency domain to the HFT recorded in the hydrothermal system at Satsuma-Iwojima (Ohiminato, 2006).

Ohiminato (2006) proposed that HFT could be generated by crack-shaped pockets filled with water. The temperature of the water in the pocket increases gradually, heated by magma or hot volcanic gas, and in time reaches the superheated state. When the temperature exceeds boiling point by a certain amount, the superheated state is broken and the water in the pocket suddenly vaporizes causing a pressure jump in the pocket. The valve opens and the gas flows out of the pocket generating HFT. After a few minutes, the pressure in the pocket decreases and the valve closes, terminating the vapour flow.

A great number of source models have been proposed to explain SDE and their dominant complex frequencies: rapid discharges of gas (Steinberg and Steinberg, 1975), oscillations of magma-filled cracks excited by crack tip extension (Chouet, 1988), resonance of a magma pipe (Chouet, 1985), oscillations of a spherical magma reservoir (Crosson and Bame, 1985; Fujita et al., 1995), periodic magma flow (Ukawa and Ohtake, 1987), acoustic emissions from collapsing bubbles (Chouet, 1992), self-excitation of a magma conduit in a manner similar to that of a flute (Julian, 1994), oscillations of a steam-filled crack by unsteady choked flow (Morrissey and Chouet, 1997), shock-tube theory (Montalto, 1993).

The signals acquired in this experiment are not sufficient to indicate a reliable source model for the Marsili area.

However, the great number and variety of signals recorded do point towards an intense hydrothermal and volcanic activity in this

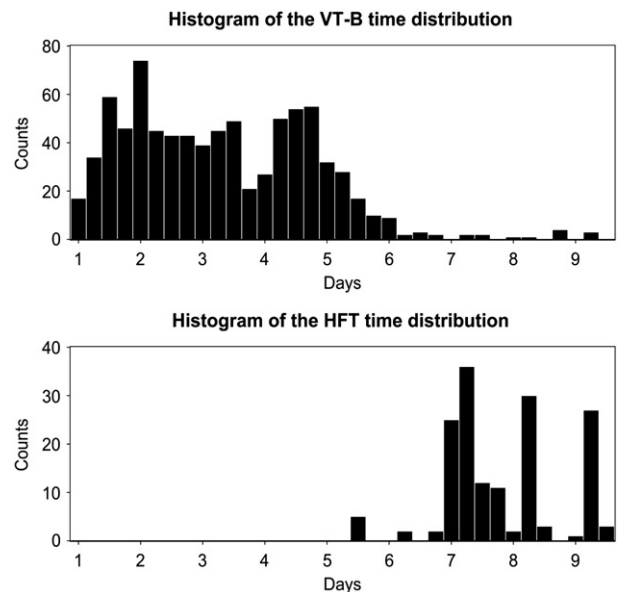


Fig. 16. Cumulative histogram with bin width of 4 h of the time distribution of the VT-B and HFT events. Throughout the first seven days, Marsili's seismic activity was characterized by the occurrence of a swarm of VT-B, the intensity of which drastically decreased during the last two days. The last two days were instead characterized by a continuous volcanic tremor, having the same spectral content and similar azimuth of the VT-B, and by a scattered occurrence of high frequency tremor.

area. These new OBS/H data open a window on Marsili's activity, nevertheless further studies are necessary to better understand the main volcanic processes that are taking place.

Acknowledgements

Our thanks go to the technicians of the Gibilmanna OBS Lab (Palermo, Sicily), Roberto D'Anna, Giuseppe Passafiume and Stefano Speciale, for their contribution to the construction, testing and deployment of the OBS/H. We are also grateful to the two anonymous reviewers for their constructive comments and suggestions.

References

- Alparone, S., Cammarata, L., Cannata, A., Gambino, S., Milluzzo, V., Gresta, S., 2008. Time-space variation of the 2004–2006 micro-seismicity at La Fossa (Vulcan, Aeolian Islands, Italy). EGU General Assembly, vol. 10.
- Argnani, A., 2000. The southern Tyrrhenian subduction system: recent evolution and neotectonic implications. *Ann. Geophys.* 43, 585–607.
- Bartosch, T., Seidl, D., 1999. Spectrogram analysis of selected tremor signals using short-time Fourier transform and continuous wavelet transform. *Ann. Geophys.* 42, 497–506.
- Beccaluva, L., Rossi, P.L., Serri, G., 1982. Neogene to recent volcanism of the Southern Tyrrhenian-Sicilian area: implications for the geodynamic evolution of the Calabrian arc. *Earth Evol. Sci.* 3, 222–238.
- Calò, M., Dorbath, C., Luzio, D., Rotolo, S.G., D'Anna, G., 2009. Local earthquakes tomography in the southern Tyrrhenian region (Italy): geophysical and petrological inferences on subducting lithosphere. *Subduction Zone Dynamics*, Springer. doi:10.1007/978-3-540-87974-9.
- Chouet, B., 1985. Excitation of a buried magmatic pipe: a seismic source model for volcanic tremor. *J. Geophys. Res.* 90, 1881–1893.
- Chouet, B., 1988. Resonance of a fluid-driven crack: radiation properties and implications for the source of long-period events and harmonic tremor. *J. Geophys. Res.* 93, 4375–4400.
- Chouet, B., 1992. A seismic model for the source of long-period events and harmonic tremor. In: Gasparini, P., Scarpa, R., Aki, K. (Eds.), *Volcanic Seismology*. Springer-Verlag, New York, pp. 133–156.
- Chouet, B., 1996. New methods and future trends in seismological volcano monitoring. In: Scarpa, R., Tilling, R. (Eds.), *Monitoring and Mitigation of Volcano Hazards*. Springer-Verlag, Berlin New York, pp. 23–98.
- Chouet, B., 2003. Volcano seismology. *Pure Appl. Geophys.* 160, 739–788.
- Crosson, R.S., Bame, D.A., 1985. A spherical source model for low frequency volcanic earthquakes. *J. Geophys. Res.* 90, 10,237–10,247.
- D'Alessandro, A., D'Anna, G., Mangano, G., Amato, A., Favali, P., Luzio, D., 2006. Evidenze sperimentali dell'attività del vulcano sottomarino Marsili. 25° Conv. Naz del GNGTS, Roma, pp. 170–172.
- D'Alessandro, A., D'Anna, G., Luzio, D., Mangano, G., 2007. Analisi spettrale parametrica e di polarizzazione applicate agli eventi sismici registrati sul vulcano sottomarino Marsili. 26° Conv. Naz del GNGTS, Roma, pp. 191–193.
- D'Alessandro, A., D'Anna, G., Luzio, D., Mangano, G., 2008. Polarization and high resolution parametric spectral analysis applied to the seismic signals recorded on the Marsili submarine volcano. EGU General Assembly, vol. 10.
- D'Anna, G., Mangano, G., D'Alessandro, A., Amato, A., 2007. The new INGV broadband OBS/H: test results on submarine volcano Marsili and future developments. EGU General Assembly, Vienna, vol. 9.
- Díaz, J., Gallart, J., Gaspà, O., 2007. Atypical seismic signals at the Galicia Margin, North Atlantic Ocean, related to the resonance of subsurface fluid-filled cracks. *Tectonophysics* 433, 1–13.
- Faggioni, O., Pinna, E., Savelli, C., Schreider, A.A., 1995. Geomagnetism and age study of Tyrrhenian seamounts. *Geophys. J. Int.* 123, 915–930.
- Flinn, E.A., 1965. Signal analysis using rectilinearity and direction of particle motion. *Porc. I.E.E.E.* 53, 1874–1876.
- Fujita, E., Ida, Y., Oikawa, J., 1995. Eigen oscillation of a fluid sphere and source mechanism of harmonic volcanic tremor. *J. Volcanol. Geotherm. Res.* 69, 365–378.
- Julian, B.R., 1994. Volcanic tremor: nonlinear excitation by fluid flow. *J. Geophys. Res.* 99, 859–877.
- Kastens, K., Mascle, J., Auroux, C.A., Bonatti, E., Broglia, C., Channell, J., Curzi, P., Emeis, K., Glacon, G., Hasegawa, S., Hieke, W., Mascle, G., McCoy, F., McKenzie, J., Mendelson, J., Mueller, C., Rehault, J., Robertson, A., Sartori, R., Sprovieri, R., Torii, M., 1988. ODP Leg 107 in the Tyrrhenian Sea: insight into passive margin and backarc basin evolution. *Geol. Soc. Amer. Bull.* 100 (1), 1140–1156.
- Konstantinos, I.K., Schlindwein, V., 2002. Nature, wavefield properties and source mechanism of volcanic tremor: a review. *J. Volcanol. Geotherm. Res.* 119, 161–187.
- Marani, M.P., Gamberi, F., 2004. Structural framework of the Tyrrhenian Sea unveiled by seafloor morphology. *Mem. Descr. Carta Geol. d'It.*, pp. 97–108. LXIV.
- Marani, M.P., Gamberi, F., Casoni, L., Carrara, G., Landuzzi, V., Musacchio, M., Penitenti, D., Rossi, L., Trua, T., 1999. New rock and hydrothermal samples from the southern Tyrrhenian Sea: the MAR-98 research cruise. *G. Geol.* 61, 3–24.
- Marani, M.P., Gamberi, F., Bonatti, E., 2004. In: Marani, M.P., Gamberi, F., Bonatti, E. (Eds.), *From Seafloor to Deep Mantle: Architecture of the Tyrrhenian Backarc Basin*. APAT.
- McCreery, C.S., Duennebier, F.K., Sutton, G.H., 1993. Correlation of deep ocean noise (0.4–20 Hz) with wind, and the Holu spectrum a worldwide constant. *J. Acoust. Soc. Am.* 93, 2639–2648.
- McNutt, S.R., 1992. In: Nierenberg, W.A. (Ed.), *Volcanic Tremor*. Encyclopedia of Earth System Science, vol. 4. Academic Press, San Diego, pp. 417–425.
- McNutt, S.R., 1996. Seismic monitoring and eruption forecasting of volcanoes: a review of the state of the art and case histories. In: Scarpa, R., Tilling, R. (Eds.), *Monitoring and Mitigation of Volcano Hazards*. Springer-Verlag, Berlin New York, pp. 99–146.
- McNutt, S.R., 2000. In: Sigurdsson, H. (Ed.), *Volcano Seismicity*. Encyclopedia of Volcanoes. Academic Press, San Diego, pp. 1015–1034.
- McNutt, S.R., 2005. Volcanic seismology. *Annu. Rev. Earth Planet. Sci.* 32, 461–491.
- Minakami, T., 1960. Fundamental research for predicting volcanic eruptions. *Bull. Earthq. Res. Inst. Tokyo Univ.* 38, 497–544.
- Mongelli, F., Zito, G., De Lorenzo, S., Doglioni, C., 2004. Geodynamic interpretation of the heat flow in the Tyrrhenian Sea. *Mem. Descr. Carta Geol. d'It.*, pp. 71–82. LXIV.
- Montalto, A., 1993. Seismic events at Vulcano (Italy) during 1988–1992. *J. Volcanol. Geotherm. Res.* 60, 193–206.
- Montuori, C., Cimini, G.B., Favali, P., 2007. Teleseismic tomography of the southern Tyrrhenian subduction zone: new results from seafloor and land recordings. *J. Geophys. Res.* 112, B03311.
- Morrissey, M.M., Chouet, B.A., 1997. A numerical investigation of choked flow dynamics and its application to the triggering mechanism of long-period events at Redoubt Volcano, Alaska. *J. Geophys. Res.* 102, 7965–7983.
- Nakano, M., Kumagai, H., Kumazawa, M., Yamaoka, K., Chouet, B.A., 1998. The excitation and characteristic frequency of the long-period volcanic event: an approach based on an inhomogeneous autoregressive model of a linear dynamic system. *J. Geophys. Res.* 103, 10031–10046.
- Neuberg, J., Luckett, R., Baptie, B., Olsen, K., 2000. Models of tremor and low frequency earthquake swarms onMontserrat. *J. Volcanol. Geotherm. Res.* 101, 83–104.
- Nicolosi, L., Speranza, F., Chiappini, M., 2006. Ultrafast oceanic spreading of the Marsili Basin, southern Tyrrhenian Sea: evidence from magnetic anomaly analysis. *Geology* 34, 717–720.
- Ohiminato, T., 2006. Characteristics and source modelling of broadband seismic signals associated with the hydrothermal system at Satsuma-Iwojima volcano, Japan. *J. Volcanol. Geotherm. Res.* 158, 467–490.
- Okada, H., 2003. The microtremor survey method. *Geophys. Monogr. Ser. Soc. Explor. Geophys.* 12, 135.
- Panza, G.F., Pontevivo, A., Saraò, A., Aoudia, A., Peccerillo, A., 2004. Structure of the lithosphere–asthenosphere and volcanism in the Tyrrhenian Sea and surroundings. *Mem. Descr. Carta Geol. d'It.*, pp. 29–57. LXIV.
- Panza, G.F., Peccerillo, A., Aoudia, A., Farina, B., 2007. Geophysical and petrological modelling of the structure and composition of the crust and upper mantle in complex geodynamic setting: the Tyrrhenian Sea and surroundings. *Earth-Sci. Rev.* 80, 1–46.
- Peterson, J., 1993. *Observation and Modeling of Background Seismic Noise*: U.S. Geol. Surv. Open-File Rept., Albuquerque, pp. 93–322.
- Pinnegar, C.R., 2006. Polarization analysis and polarization filtering of three-component signals with the time-frequency S transform. *Geophys. J. Int.* 165, 596–606.
- Piromallo, C., Morelli, A., 2003. P-wave tomography of the mantle under the Alpine-Mediterranean area. *J. Geophys. Res.* 108, 2065.
- Sartori, R., 1989. Evoluzione neogenico-recente del bacino tirrenico e i suoi rapporti con la geologia delle aree circostanti. *Giorn. Geol.* 51, 1–39.
- Sartori, R., 2003. The Tyrrhenian back-arc basin and subduction of the Ionian lithosphere. *Episodes* 26, 217–221.
- Seidl, D., Hellweg, M., Rademacher, H., Gómez, D.M., Torres, R.A., 1999. The anatomy of a tornillo: puzzles from three-component measurements at Galeras volcano (Colombia). *Ann. Geophys.* 42, 355–364.
- Steinberg, G.S., Steinberg, A.S., 1975. On possible causes of volcanic tremor. *J. Geophys. Res.* 80, 1600–1604.
- Trua, T., Serri, G., Rossi, P.L., 2004. Coexistence of IAB-type and OIB-type magmas in the southern Tyrrhenian back-arc basin: evidence from recent seafloor sampling and geodynamic implications. *Mem. Descr. Carta Geol. d'It.*, pp. 83–96. LXIV.
- Ukawa, M., Ohtake, M., 1987. A monochromatic earthquake suggestion deep-seated magmatic activity beneath the Izu-Oshima volcano, Japan. *J. Geophys. Res.* 92, 649–663.
- Wasserman, J., 2002. In: Bormann, P. (Ed.), *Volcano Seismology*, New Manual of Seismological Observatory Practice.
- Webb, S.C., 1998. Broadband seismology and noise under the ocean. *Rev. Geophys.* 36, 105–142.
- Welch, P.D., 1967. The use of the fast Fourier transform for the estimation of power spectra: a method based on time averaging over short modified periodograms. *IEEE Trans. Audio Electroacoust.* 15, 70–73.
- Wenz, G.M., 1962. Acoustic ambient noise in the ocean: spectra and sources. *J. Acoust. Soc. Am.* 34, 1936–1956.
- Yokoyama, Y., Kumazawa, M., Imanishi, Y., Mikami, N., 1997. A new method of non-stationary time series analysis based on inhomogeneous AR equation, *IEEE trans. Signal Process.* 45, 2130–2136.
- Zito, G., Mongelli, F., de Lorenzo, S., Doglioni, C., 2003. Geodynamical interpretation of the heat flow in the Tyrrhenian Sea. *Terra Nova* 15, 425–432.
- Zobin, V.M., 2003. *Introduction to Volcanic Seismology*. Elsevier Publications, Amsterdam.